Article:
Yildirim, C., Ulus, H. orcid.org/0000-0001-8591-8993, Sas, H.S. orcid.org/0000-0002-5179-2509 et al. (2 more authors) (2025) Assessing the fracture and dynamic mechanical performance of CF/PEKK joints bonded with epoxy-based adhesive film for aerospace applications: impact of thermal and cycling hygrothermal conditions. Composites Part A: Applied Science and Manufacturing, 190. 108659. ISSN 1359-835X

https://doi.org/10.1016/j.compositesa.2024.108659

Assessing the Fracture and Dynamic Mechanical Performance of CF/PEKK Joints Bonded with Epoxy-based Adhesive Film for Aerospace Applications: Impact of Thermal and Cycling Hygrothermal Conditions

Ceren Yildirim [a,b], Hasan Ulus [a,c], Hatice S. Sas [a,b,d], Serra Topal [a], Mehmet Yildiz [a,b] *

[a] Sabanci University Integrated Manufacturing Technologies Research and Application Center & Composite Technologies Center of Excellence, Manufacturing Technologies, Istanbul 34906, Turkiye

[b] Faculty of Engineering and Natural Sciences, Sabanci University, Tuzla, Istanbul 34956, Turkiye

[c] Selcuk University, Huglu Vocational School, Konya 42700, Turkiye

[d] School or Mechanical, Aerospace and Civil Engineering, The University of Sheffield, S1 3JD, UK

* Corresponding author. e-mail:mehmet.yildiz@sabanciuniv.edu

Abstract

This comprehensive study evaluates the performance of advanced thermoplastic composites' adhesively bonded joints (ABJs), focusing on fracture toughness and dynamic-mechanical analysis (DMA) across a wide range of environmental conditions: room temperature (RT), low temperature (LT), high temperature (HT), and cyclic hygrothermal (CHT). Fracture toughness of ABJs are assessed using double cantilever beam (DCB) and end-notched flexure (ENF) tests. Moreover, extensive efforts to bridge the gap in understanding fracture failure behavior, using acoustic emission (AE) monitoring, detailed stereo microscopy, and scanning electron microscopy (SEM), achieve a comprehensive understanding of the effects of various environmental conditions. Results indicate that HT and CHT conditions significantly reduce both mode-I and mode-II fracture toughness compared to RT, whereas LT conditions enhance mode-II toughness despite decreasing mode-I toughness. ENF and DMA results consistently demonstrate that LT-conditioned specimens exhibit the highest performance, whereas HT-conditioned specimens demonstrate the lowest. The combined effects of thermal cycling and moisture in CHT conditions lead to intermediate storage modulus and a reduced glass transition temperature (T_g) of adhesive film. The novel findings exhibit the critical role of environmental factors in designing ABJs for aerospace applications, aiming to optimize performance and reliability under varying operational conditions.

Keywords: adhesively bonded joints; environmental conditions; fracture toughness; acoustic emission inspection

Abbreviations and nomenclature

ABJ	Adhesively bonded joint	**HDT**	**Hit definition time**
ADH	Adhesive failure	**HPTPC**	High-performance thermoplastic composites
AE	Acoustic emission	**HT**	High temperature
AF	Adhesive film	**KFF**	Knitted fiber failure
APA	Atmospheric plasma activation	**LAFP**	Laser-assisted automated fiber placement
CF	Carbon fiber	**LFT**	Light fiber tear failure
CFF	Carbon fiber failure	**LT**	Low temperature
CFRP	Carbon fiber reinforced plastic	**MC**	Matrix cracking
CHT	Cyclic hygrothermal	**NDT**	Nondestructive testing
COH	Cohesive failure	**PEKK**	polyether-ether-ketone-ketone
CTE	Coefficients of thermal expansion	**RH**	Relative humidity
DCB	Double cantilever beam	**RT**	Room temperature
DMA	Dynamics mechanical analysis	**SEM**	Scanning electron microscopy
ENF	End-notched flexure	**SFE**	Surface free energy
EHT	Electron high tension	**SHM**	Structural health monitoring
$\mathbf{G_{IC}}$	Mode-I interlaminar fracture toughness	$\mathbf{T_g}$	Glass transition temperature
$\mathbf{G_{IC\text{-}init}}$	Mode-I interlaminar fracture toughness of the initiation region	**TLC**	Thin-layer cohesive failure
$\mathbf{G_{IC\text{-}prop}}$	Mode-I interlaminar fracture toughness of the propagation region	**WB**	Wideband
HLT	Hit lockout time		

1. Introduction

High-performance thermoplastic composites (HPTPCs) have gained significant attention in aerospace applications owing to their superior advantages including high damage tolerance, chemical stability, impact resistance. Adhesively bonded joints (ABJs) have emerged as a critical technique for assembling HPTPC structures, offering advantages such as weight reduction, improved fatigue resistance, enhanced structural integrity, compared to traditional methods like mechanical fastening or fusion bonding [1–3]. However, surface treatment plays a significant role in achieving high bonding quality by establish appropriate surface conditions characterized by the desired levels of roughness, surface free energy (SFE), and wettability [4]. In comparison to traditional treatment methods such as solvent cleaning, peel-ply treatment, sanding, chemical etching, and blasting techniques, atmospheric plasma activation (APA) offers several notable advantages. With APA, the surface is treated by forming polar groups such as carbonyl, carboxyl, and hydroxyl on the surface of the adherend, leading to an augmentation in SFE and roughness. Consequently, APA has become increasingly favored as a surface treatment method, largely due to its numerous advantages, including cost-effectiveness, shortened processing time, wide field application, environmentally and healthily friendly, and uniform adhesion properties [5,6]. While

the potential advantages of ABJs have sparked growing interest in the industry, concerns arise regarding their durability and long-term performance under operating conditions [7].

The aerospace industry presents exceptionally challenging operational conditions, where composite materials used for aircraft structural components encounter a variety of demanding chemical and physical environmental factors during service [8–10]. These factors include extreme temperatures, humidity, UV radiation, chemical exposure, and mechanical stresses, all of which can impact the performance and longevity of the materials. Among these, temperature changes significantly impact the strength and fracture behavior of ABJs due to alterations in adhesive performance and residual stresses at the interface, resulting from differences in the coefficients of thermal expansion (CTE) of their components [11]. Elevated temperatures reduce adhesive strength, while lower temperatures induce high thermal stresses and increase adhesive brittleness. At higher temperatures, softening of the resin matrix and adhesives leads to an increased viscoelastic response, primarily impacting the properties of the resin matrix. Conversely, at lower temperatures, which simulate cryogenic conditions, the matrix exhibits increased brittleness, resulting in reduced mechanical performance, particularly in Mode-I fracture toughness.

Additionally, cycling hygrothermal loading simulates real-world conditions encountered in aerospace operations, such as those experienced during the takeoff and landing phases of aircraft. This loading regime has the potential to significantly degrade the performance of ABJs due to the combined disruptive effects of temperature and moisture [12,13]. Moisture initiates plasticization and swelling in both the adhesive matrix and the matrix phase of composite laminates [14]. This leads to a weakened interface both adhesive-adherend and adhesive-supporting carrier of adhesive. Additionally, combination of moisture absorption, CTE and thermal shock can create residual stresses within the ABJs [15]. Therefore, the influence of temperature and moisture on the strength and fracture toughness of ABJs is a crucial factor that must be considered for optimizing design and material selection for specific applications.

Adhesively bonded composite joints in service often face a range of loading conditions, including opening (mode-I) and sliding (mode-II) forces, which are critical for assessing the fracture toughness of these joints. Failure to adequately address these stresses can inflict severe damage on the primary structure, potentially leading to catastrophic failure [16,17]. Thereby, the literature includes studies that provide experimental results particularly on the fracture toughness of ABJs under various environmental conditions. Banea et al. [18,19] have studied the effects of temperature on the fracture toughness of ABJs under mode-I and mode-II loading conditions. They have found that the fracture-strength, -stress, and -toughness of ABJs are temperature-dependent. Their results indicate that fracture toughness increases up to the T_g, but decreases abruptly and significantly at

temperatures above T_g. Ashcroft et al. [20] have investigated the effect of temperature on epoxy-bonded carbon fiber reinforced plastic (CFRP) joints at -50°C, 22°C and 90°C. The highest (1500 J/m^2) and lowest (250 J/m^2) opening mode-I interlaminar fracture toughness (G_{IC}) are obtained at 90°C and -50°C, respectively. Fractures in the composite observed at LT become cohesive failure as the temperature increases, thereby increasing the fracture energy. Yoshimura et al. [21] have also emphasized a significant reduction in mode-I fracture toughness of adhesively bonded CFRP joints characterized by DCB tests at LT, attributed to a shift in fracture behavior from cohesive to adhesive failure. In contrast, ENF test results have revealed that mode-II fracture toughness increases at LT compared to RT. Similarly, Melcher et al. [22] have reported an approximately 58% reduction in mode-I fracture toughness for ABJs with thermoset-based adherends at LT compared to those at RT. Monsef et al. [23] have assessed the effect of temperature on the fracture toughness of secondary bonded CFRP joints using two types of adhesive films. The DCB test results, conducted at −55°C, RT, and 80°C, have showed that the adhesive films become more brittle at LT, leading to unstable crack propagation and reduced fracture toughness. Additionally, both adhesive films have demonstrated that high temperature (80°C) also affects the fracture toughness of the joints. Brito et al. [24] have conducted experimental characterization of the mode-I of ABJs manufactured through co-cured and co-bonded processes under various environmental conditions, including temperatures of 25°C and -55°C. Specimens tested at RT (25°C) and LT (-55°C) show consistent outcomes across both manufacturing methods. Load-opening displacement curves indicates a reduction in maximum load as temperature decreased, with a noticeable abrupt crack propagation observes at LT. Additionally, G_{IC} declines with decreasing temperature under both productions due to the presence of temperature and moisture which affect the joint performance. Katsiropoulos et al. [25] have characterized the effect of thermal aging (as a cyclic thermal conditioning between -55°C and 80°C) and, wet aging with different adhesive type and thickness on the fracture toughness (mode-I and mode-II) experimentally. In addition to the observed strong dependence on adhesive thickness, the thermal aging and wet aging process significantly alters the G_{IC} performance of ABJs. Nevertheless, the literature lacks information on the examination of fracture toughness under a broader range of environmental conditions that more accurately represent real-life operational scenarios, particularly for thermoplastic adherends.

Moreover, nondestructive testing (NDT) methods, particularly acoustic emission (AE), are effectively used for ABJs to monitor structural integrity, identify dominant damage types and failure modes, and correlate these factors with joint performance. Specifically, during double cantilever beam (DCB) tests, AE inspection has been widely applied in research. For example, Freitas et al. [26] have used AE methods to obtain distinct AE signals associated with different characteristics of crack propagation at the interface and within the adhesive layer. Droubi

et al. [27] have employed AE technique to examine the impact of bond quality on the failure process of ABJs. Lima et al. [28] have investigated the effect of different stacking sequences of composite adherends using the AE approach to identify fracture mechanisms in ABJs. More recently, Yildirim et al. [5] and Liu et al. [29] have demonstrated the successful application of AE inspection for damage assessment in ABJs with both thermoplastic and thermoset adherends, respectively, during mode-I and mode-II tests. These studies comprehensively analyze the passive and dynamic characteristics of stress waves generated by crack movement, offering real-time monitoring of damage occurrence and propagation in ABJs. However, there remains a gap in the literature regarding the understanding of fracture toughness behavior, damage progression, and the identification of damage types in ABJs under various environmental conditions using AE inspection.

Despite extensive research on thermoset-based composite materials and adhesive bonding techniques, there remains a need to comprehensively investigate the fracture toughness behavior of adhesively bonded thermoplastic composite joints under diverse service conditions. This study aims to fill this gap by investigating the fracture toughness behavior and sophisticated failure characterization of thermoplastic-based ABJs under different environmental conditions, including room temperature (RT), low temperature (LT), high temperature (HT), and cycling hygrothermal (CHT). By systematically evaluating the influence of these environmental factors on joint integrity, this research seeks to provide valuable insights into the performance and reliability of bonded composite structures in diverse operating environments.

2. Materials and Experimental Methods

2.1 Materials

For the manufacturing of the thermoplastic composite laminates as the adherend, Toray Cetex® TC1320 unidirectional carbon-fiber (CF) reinforced polyether-ether-ketone-ketone (PEKK) semi-preg slitted tape, featuring a nominal thickness of 0.15 mm and a width of 6.35 mm, is procured from Toray Advanced Composites, USA. The constituents of the slit tape are unidirectional CF (AS4D 12K) and semi-crystalline PEKK. The fiber areal weight measures 300 g/m^2, accompanied by a resin content of 34 weight percentage (wt%). The Scotch-Weld AF 163–2K structural adhesive film (3M Company), a thermoset-based adhesive in film form with a knit supporting carrier and a nominal thickness of 0.241 mm, is used to prepare the ABJs. Extra pure isopropyl alcohol (>99.5% purity, Tekkim Chemistry, Ltd) is used as solvents to clean the adherend surfaces. The non-perforated teflon film (commercial code WL52000B, Airtech), with a thickness of 20 μm, is used as a crack tip insert to facilitate controlled crack initiation and propagation in fracture toughness testing.

2.2 Experimental Procedure

2.2.1 Specimen preparation

The CF/PEKK composite laminates with a $[0°]_{16}$ stacking sequence are manufactured using the laser-assisted automated fiber placement (LAFP) system (Coriolis C1), ensuring precise fiber placement. This is followed by autoclave consolidation to achieve optimal mechanical properties and minimal void content. The interested reader may refer to the references for a detailed account of CF/PEKK laminate manufacturing [30]. In previous study conducted by the authors, the average fiber volume fraction and void content of CF/PEKK adherends are found to be 57.47% and 0.46%, respectively, based on tests performed according to ASTM D792 standard, Method B [30].

The APA treatment is conducted using the OpenAir® FG 5001 atmospheric plasma equipment (Plasmatreat GmbH, Steinhagen, Germany) with a 25 mm nozzle diameter. Optimal parameters from our previous studies [5,6] are applied, including a nozzle distance of 15 mm, a scan speed of 40 mm/s, and a total of three scans. Before applying the APA, the adherend surfaces are cleaned with isopropyl alcohol (IPA) to remove contaminants and are air-dried in a controlled environment. After subjecting the specimens to APA treatment, the pre-conditioned adhesive films (AFs) are affixed onto the adherends and cured (at 120°C for 2h), following the procedure described in our previous study [6]. This process prepares the specimens for fracture toughness tests and dynamic mechanical analyses. The preparation of the double cantilever beam (DCB) specimen for mode-I tests (**Figure 1a**) and the end notched flexural (ENF) specimen for mode-II tests (**Figure 1b**) follows ASTM D5528 [31] and ASTM D7905 [32] standards, respectively. The specimens for dynamic mechanical analysis (DMA) tests are prepared as illustrated in **Figure 1c**. In these specimens, the adherend dimensions specified in the lap-shear test (ASTM D1002 [33]) are reduced by half to ensure the specimen is aligned parallel to the horizontal plane of the testing machine, with tabs included.

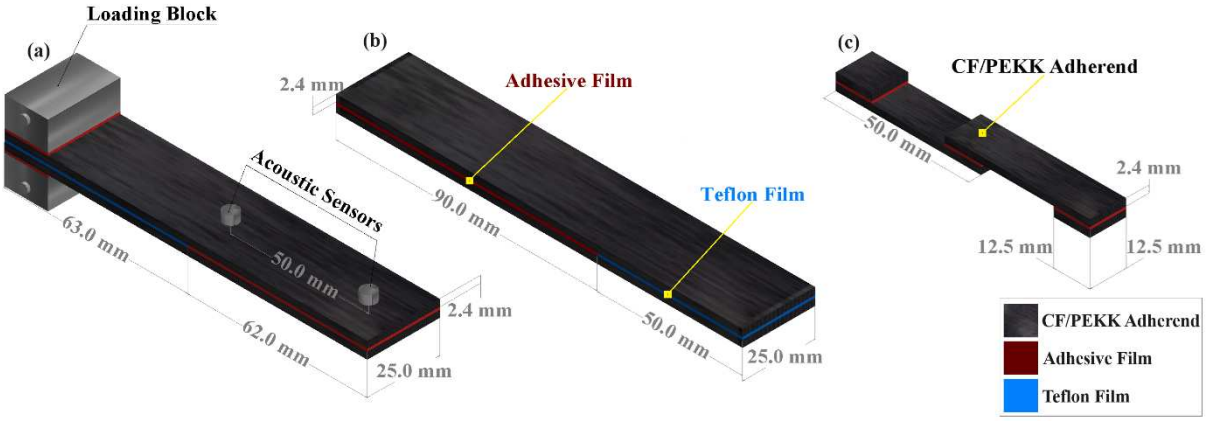

Figure 1 Schematic representation of ABJs specimens for (a) DCB, (b) ENF, and (c) DMA tests.

2.2.2 Artificial environmental conditions

Four distinct thermal condition scenarios are designed to mimic service circumstances for adhesively bonded CF/PEKK composite joints, as outlined in **Table 1**. These scenarios aim to evaluate the joints' performance under the following conditions: i. room temperature (RT), ii. high temperature (HT), iii. low temperature (LT), and iv. cycling thermal conditions. The first set, which is allowed to rest at RT (approximately 25°C) for 1 hour after the curing process, is tested under ambient conditions. The second and third sets are exposed to low (-40 °C) and high (70°C) temperatures for 1 hour in the climatic chamber of INSTRON 5982 universal testing machine (**Supplementary Figure S1**) and Mettler Toledo DMA/SDTA861^e instrument [34]. The fourth set is subjected to the D4 cycle in a climatic chamber (Vötsch, VC3 7150) in accordance with EN ISO 9142 [35]. The D4 cycle involves a sequence of humid-heat and cold phases, designed to simulate thermal shock and humidity effects on the ABJs, providing insights into their long-term performance under fluctuating environmental conditions. According to the ISO 9142 D4 cycle [35], the specimens are heated to 70°C and held for 5 hours at 90% relative humidity (RH). Subsequently, they are cooled to -40°C and held for 5 hours without RH control. This sequence constitutes one cycle, with each cycle taking approximately 12 hours. The total number of cycles is around 120 (see in **Table 1)**. The mass gain has been measured an increase of 0.2% at the end of the 60-day CHT conditioning period. This finding is consistent with the results of Sukur et al. [36], which shows that AFP-manufactured and autoclave-consolidated CF/PEKK laminates reaches saturation within one month of hygrothermal aging.

Table 1. Thermal conditioning scenarios of adhesively bonded CF/PEKK joints.

	Room Temperature (RT)	**High Temperature (HT)**	**Low Temperature (LT)**	**Cycling Hygrothermal (CHT)**
Environmental Condition	25 °C	70 °C	-40 °C	70 °C (90% RH) ↔ -40 °C (0% RH)
Duration	1 hour	1 hour	1 hour	60 days (~120 cycles)

2.2.3 Fracture toughness tests and dynamic mechanical analyses

To identify the effect of service condition on the delamination resistance of the ABJs, mode-I and mode-II fracture toughness are investigated followed by ASTM D5528 and ASTM D7905 standards of INSTRON 5982 universal testing machine with a 100 kN load cell. Tensile force is applied to aluminum loading blocks affixed to the ends of the DCB specimens to initiate crack propagation. Crack propagation in DCB specimens, whose side surfaces are marked with straight lines to aid in monitoring crack propagation, is visually monitored using a 10X LED magnifier and real-time of results is recorded by integrated button on the testing apparatus. To determine the characteristics of defects in stress waves caused by sudden crack movement during mode-I test, real-time comprehensive monitoring of damage accuracy and propagation in ABJs is conducted using the Mistras PCI-2 AE system with two wideband (WB) sensors attached to the specimen surface. Signal quality is enhanced using two preamplifiers with 20 dB gain and analog filters operating between 1 kHz and 3 MHz, with a 45 dB threshold value applied to eliminate ambient noise. The AE parameters are configured as follows: peak definition time (PDT) = 50 μs, hit definition time (HDT) = 150 μs, hit lockout time (HLT) = 300 μs, and maximum duration = 100 μs. The sample rate, trigger value, and hit length value are determined to be 2 MSPS, 100 μs, and 2 K, respectively.

Dynamics mechanical analysis (DMA) is performed on joint specimens (**Figure 1c**) exposed to four different thermal conditions to reveal the dynamic-mechanical behavior of ABJs. The DMA tests are conducted using a Mettler Toledo DMA/SDTA861^e instrument in 3-point bending mode (to be able to correlate with finding of ENF tests [37]), at a frequency of 1.00 Hz and a heating rate of 3°C/min. The RT specimens and CHT specimens (conditioned in the climatic chamber) are tested within the temperature range of 25°C to 250°C. The LT and HT specimens, which are conditioned in the DMA instrument at -40°C and 70°C respectively, are tested up to 250°C. These specimens are allowed to equilibrate at their respective temperatures for 1 hour each before testing begins, with the tests starting at these temperatures.

2.2.4. Fracture surface examination

Two distinct microscopy techniques are employed to assess the impact of service conditions on the fracture surface, damage classification, and interfacial morphology of ABJs. Macro images are captured using a Nikon SMZ800N Stereo microscope. Detailed surface morphologies are conducted utilizing a Zeiss Leo Supra VP35 scanning electron microscopy (SEM), operated at an electron high tension (EHT) voltage of 5 kV and a working distance of 12-16 mm range. The secondary electron detector is selected for generating SEM images.

3. Results and Discussion

3.1 Opening Mode (mode-I) Results

Representative load versus crack opening displacement curves for DCB samples conditioned under different environmental conditions are presented in **Figure 2a** and photographic images showing the failure behaviors are provided in **Figure 3**. The load-displacement curves for RT, HT, and CHT conditioned specimens show minimal sharp peaks, indicating a transition from unstable to stable crack propagation compared to LT specimens' curve. This is characterized by slower and more controlled crack propagation with frequent load drops. This behavior can be attributed to the inherent viscoelastic properties of the adhesive, which cause thermal stresses to dissipate rapidly [15]. Specifically, under HT conditions, the adhesive film (AF) exhibits increased ductility [12], promoting easier crack propagation and smoother load drop-offs. These findings, which show higher load values in the load-displacement curves during the initial stage of critical crack propagation compared to LT, are supported by photographic images of specimens conditioned at RT, HT, and CHT (**Figure 3a,b,d**). The images indicate fiber debonding and bridging under load. However, the increased ductility of the adhesive matrix at HT facilitates easier debonding of the knitted supporting carrier, as shown in **Figure 3b**, suggesting that this AF may not be effective for load-bearing at elevated temperatures.

In LT-conditioned specimens, a notable difference among the other specimens is the distinct peak load observed at the beginning of delamination propagation. These cold-exposed specimens frequently exhibit adhesive stick-slip behavior, characterized by a load increase without crack growth, followed by a sudden and sharp load drop due to unstable crack propagation (see **Figure 3c**) [5]. This delay in crack propagation is caused by the absorption of elastic energy within the system. Once the absorbed energy exceeds the threshold required for crack propagation, the delamination process resumes until the energy is depleted, resulting in an unstable crack propagation pattern. Unlike thermoset-based ABJs, which exhibit stable and brittle fractures at LT and discontinuous crack growth with stick-slip behavior at RT, thermoplastic-based ABJs show stable crack propagation at RT and stick-slip crack growth at LT [20].

The load-displacement curve of CHT-conditioned specimens exhibits a trend akin to those of RT and HT-conditioned counterparts, yet with a notable distinction: its maximum load value falls between that of RT and HT-conditioned ones. This suggests a nuanced response to the combined thermal and humidity conditions. Thermal cycling and humidity at 70°C can prompt several effects on the adhesive layer including both adhesive polymer and knitted fibers. For example, humidity is prone to infiltrate existing voids in the adhesive, causing internal expansion and the formation of micro-cracks due to thermal shock [14]. These cracks may then coalesce,

impacting the structural integrity of the joint. Additionally, the absorbed moisture may cause weakening of the interface between the knitted fiber-adhesive polymer, resulting in segregation and/or knitted fiber failure (KFF), including bridging and breakage tendencies (**Figure 3d**). As a result of these factors, CHT-conditioned specimens exhibit lower delamination resistance than the RT-conditioned ones, but higher than the HT-conditioned specimens. The presence of ambient humidity may induce swelling of the adhesive, typically resulting in negligible residual stresses within the ABJs as a consequence of its plasticizing influence, but it can also contribute to the mitigation of thermal stresses [15]. Therefore, CHT samples group demonstrate reduced strength in contrast to those held at RT, yet display heightened strength relative to specimens exposed to HT conditioning. Average maximum load values are 283.09±1.20 N (RT), 202.18±5.45 N (HT), 160.03±10.05 N (LT) and 216.99±2.0 N (CHT). The results show that thermoplastic-based ABJs exhibit higher delamination resistance compared to thermoset-based ABJs in different environmental conditions [25,38].

Additionally, representative G_{IC} versus crack growth curves of different conditioned joints are shown in **Figure 2b**. Following the modified beam theory specified in ASTM D5528, the average G_{IC} fracture toughness values for RT, HT, LT, and CHT-conditioned joints are calculated and presented as initiation and propagation region as shown in the inset bar chart (**Figure 2b**). However, propagation region of the LT specimen presents an unstable crack growth, meaning the real curve at equilibrium exhibits snap-back instability (**Figure 2b**). Moreover, for LT specimens, a reliable data set is available for $G_{IC\text{-}init}$ values, while $G_{IC\text{-}prop}$ is not considered due to a lack of data points. The results in **Figure 2b** show that the fracture toughness of ABJs is strongly influenced by environmental conditions, with both $G_{IC\text{-}init}$ and $G_{IC\text{-}prop}$ values highlighting this, even in the LT case where propagation data are not considered. Specifically, it is observed that the mode-I toughness significantly decreases at LT, consistent with literature findings [22]. Contrary to assertions in the literature [20], however, it is noted that the fracture toughness can also diminish with rising temperatures. This can be explained by the peel-off behavior of knitted supporting carriers from the adhesive matrix, which becomes more ductile at HT (**Figure 3b**). In addition, it is presumed that the load-carrying capability of the knitted supporting carriers decreases due to the temperature, causing crack growth before reaching high load values.

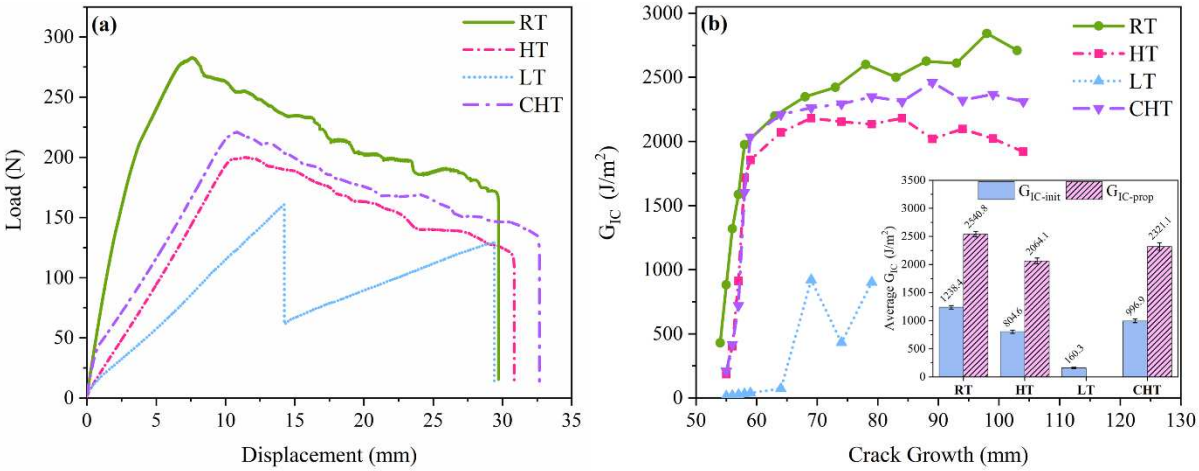

Figure 2 Mode-I fracture toughness test results: (a) Load-displacement curves and (b) fracture resistance curve with an inset bar chart for initiation and propagation regions.

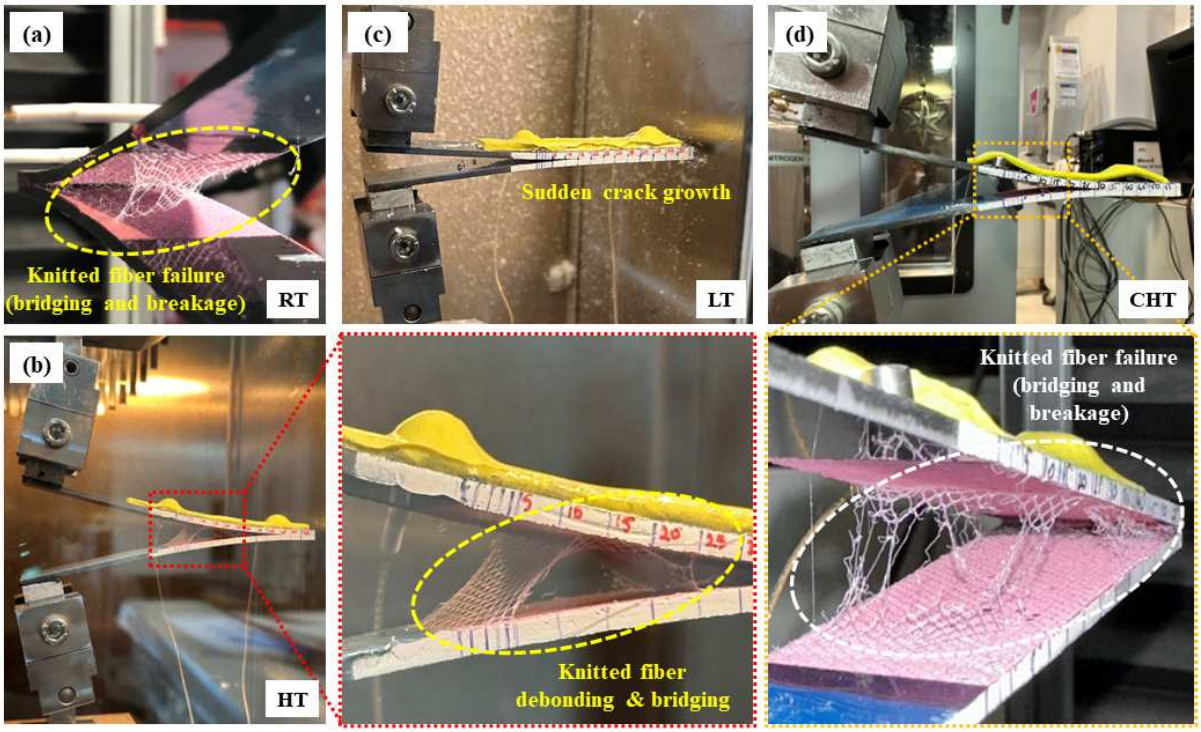

Figure 3 (a-d) Photographic images depicting fracture behaviors of DCB specimens tested under RT, HT, LT, and CHT conditions, respectively.

3.1.1 Acoustic emission inspection

The application of the K-means clustering technique yields classification results for representative joints, as illustrated in **Figure 4**, which also includes inset pie charts showing the percentage distributions of failure modes under different environmental conditions. The outcomes reveal five distinct damage clusters characterized by different frequency ranges, namely 0-100 kHz, 100-180 kHz, 180-400 kHz, 400-550 kHz, and 550-750 kHz [5]. The initial cluster (C1), encompassing the lowest frequency range (0-100 kHz), is associated with adhesive failure (ADH) and/or matrix cracking (MC). Cluster two (C2) and cluster four (C4) are linked to adhesive peeling

and/or light fiber tear failure (LFT). Specifically, C2 (100-180 kHz) pertains to thin-layer cohesive failure (TLC), while C4 (400-550 kHz) is affiliated with cohesive failure (COH) and/or LFT. Furthermore, the third cluster (C3) within the range of 180-500 kHz is correlated with the debonding of the supporting carrier (knitted fiber), while the fifth cluster (C5) falls under the category of carbon fiber failure (CFF) and/or knitted fiber failure (KFF) in the form of bridging and breakage.

ABJs consist of different materials, namely AF and adherend, each with various coefficients of thermal expansion (CTE). Given the high strength and modulus of CF, CF-reinforced composites exhibit a very low CTE [39]. As the temperature rises, the adhesive, having a higher CTE, expands more than the adherend, exerting tensile stresses on the adhesive layer. If the adhesive cannot withstand these stresses, COH within the adhesive itself may occur. Additionally, there can be a mismatch in thermal expansion between the adhesive matrix and knitted fiber, resulting in the development of misfit strain at the knitted fiber-adhesive resin interface, leading to debonding [40]. These thermal effects contribute to the observed differences in acoustic emission (AE) inspection findings. Comparing the AE inspection findings for RT and HT, at elevated temperatures, this debonding is anticipated to occur more readily, thereby promoting delamination or cracking from the central region of the film as shown in **Figure 3** and later to be confirmed with SEM analysis. As the adhesive matrix becomes more ductile, the delamination progression can occur easily. Thus, the proportion of C1 and C2 failures decreases, while C4 failures increase with heat application to ABJs. Consequently, it is expected that there will be an augmentation in the proportion of COH. Moreover, due to this easy separation, the crack propagates before the knitted fibers reach the load-bearing point, hence reducing the damage from 0.79% to 0.57% (refer to **Figure 4a,b**).

Nonetheless, materials tend to contract upon decreased thermal energy in cryogenic conditions. When ABJs are cooled to low temperatures (-40 °C), the adhesive and adherends undergo contraction at different rates due to their distinct CTE values [41]. Hence, when cooling ABJs down from ambient temperature to LT, different amounts of thermal contractions are occurred for AF and composite laminates. These differential contractions result in the development of compressive stresses within the AF, as it tries to shrink more than the adherends can accommodate. This can apply tensile stress to the adherend surface. At LT, the AF, prone to greater shrinkage which can induce partial detachment from the matrix due to microcracking effect, particularly as the matrix becomes brittle under stress. This phenomenon, known as light fiber-tear failure (LFT), is exacerbated by weakened adhesion at the fiber-matrix interface, a consequence of cryogenic-induced matrix brittleness, which further triggers mechanisms such as fiber-matrix debonding or interfacial failure [24,34]. For these reasons, the dominant failure modes are COH and/or LFT. Triggered interfacial failure can lead to fractures in the composite

fibers, resulting in an increased percentage in C5 compared to RT and HT-conditioned specimens. Also, the total AE hits decrease for LT conditioned specimens due to the sudden crack, as expected (see in **Figure 4c**).

Thermal cycling may induce material degradation and alterations in constituent material properties, potentially compounded by additional hygroscopic effects. These changes can influence the overall macroscopic properties of ABJs [42]. The cumulative impact of thermal effects may have notable long-term consequences on the material behavior, leading to different failure types and percentages compared to other conditions. For example, thermal cycling affects both the matrix of the composite and the adhesive polymer, potentially increasing MC in both polymer types. This is supported by the observation that thermal cycling results in both ductile and brittle fracture mechanisms [42]. Moreover, the interaction between the AF and the adherend can weaken due to the presence of humidity and differences in the CTE. As a result, the percentage of C1 failure attributed to MC and/or ADH is higher than under all other condition types. Knitted fibers can also be affected by thermal cycling in terms of mechanical strength, leading to changes in the associated damage mechanisms. Evidence of this is seen in the increased percentage distribution of C5 failures when subjected to thermal cycling, which results in a corresponding decrease in debonding failure (C3) percentage due to prematurely degraded fibers compared to RT and HT conditions (see **Figure 4d**). Material degradation and CTE differences can cause interfacial failure in the adherend itself and COH in the AF, increasing AE activities associated with C4 failures under thermal cycling conditions.

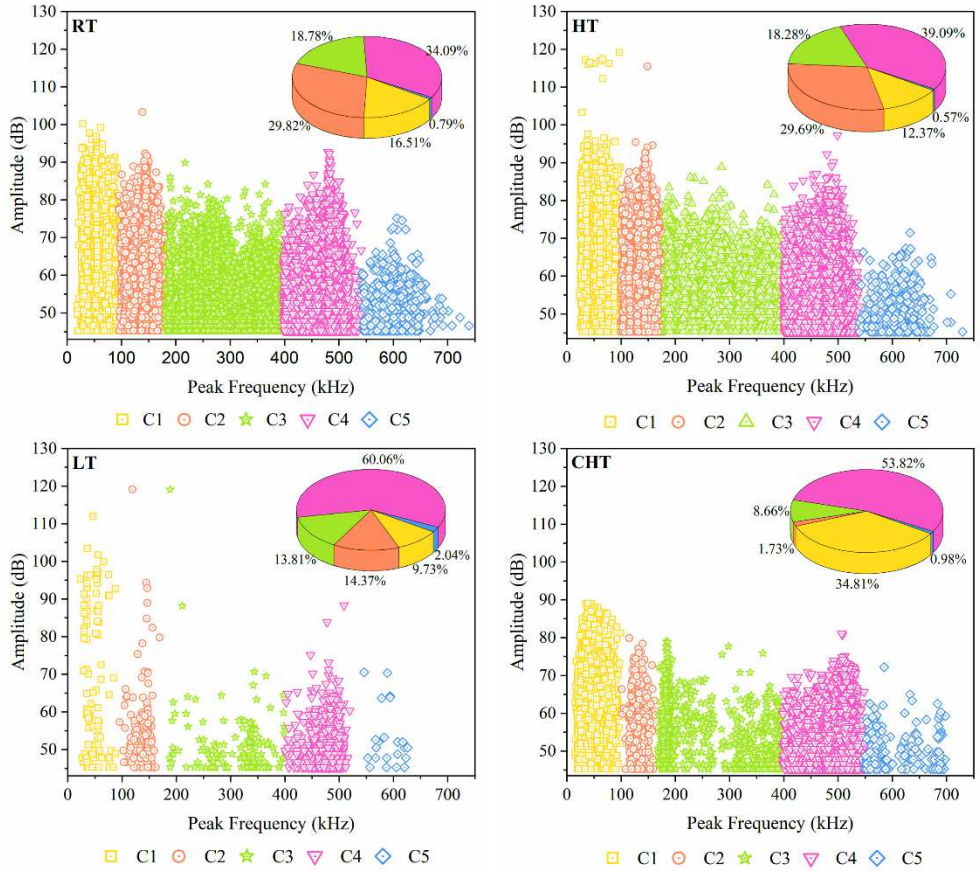

Figure 4 Variations of amplitude versus peak frequency of DCB specimens during mode-I tests with inset pie chart showing the percentage distribution of damages at RT, HT, LT and CHT conditions.

3.1.2 *Failure surfaces examination*

Fractographic failure analysis of ABJs exposed to different environmental conditions using stereo microscopy is given in **Figure 5-6.** The sharpest distinction between specimens exposed to various environmental conditions is that the LT-conditioned specimens stand out with unique fracture characteristics. However, upon individual evaluation of microscopy images of RT, HT and CHT, distinct differences become apparent among them as well. The stereo microscope analysis of RT-conditioned ABJs shows that dominant failure is COH with partial TLC, which means that the crack propagation occurs within the AF (see in **Figure 5a**). This is also supported by the observation of knitted fiber imprints and knitted fibers on the fracture surfaces. Also, KFFs are seen on the fractured surface, besides knitted fiber debonding. This microscopic observation of the RT specimen's fracture surface aligns with the AE findings, showing maximum percentage distributions of COH (C4) and TLC (C2) at 34.09% and 29.82% (**Figure 4a**), respectively.

The fracture surface analysis of HT-conditioned ABJs in **Figure 5b** reveals behavior similar to that of RT-conditioned ABJs with dominant COH and TLC, as supported by AE findings in **Figure 4b**. However, a noticeable difference in the surface appearance of HT-conditioned specimens is observed, particularly in the color

of the AF, due to the effects of temperature. It is clearly seen that the AF conditioned at HT displays a distinct color difference compared to the RT-conditioned specimen, emphasizing the presence of a yielded adhesive matrix and indicating a ductile fracture morphology (**Supplementary Figure S2**). Additionally, damaged knitted fibers are slumped down on the surface, indicating that the fibers have also been ductilized by the temperature. This can be observed from the decrease in the percentage distribution in MC (C1) from AE findings to 12.37% compared to corresponding RT findings.

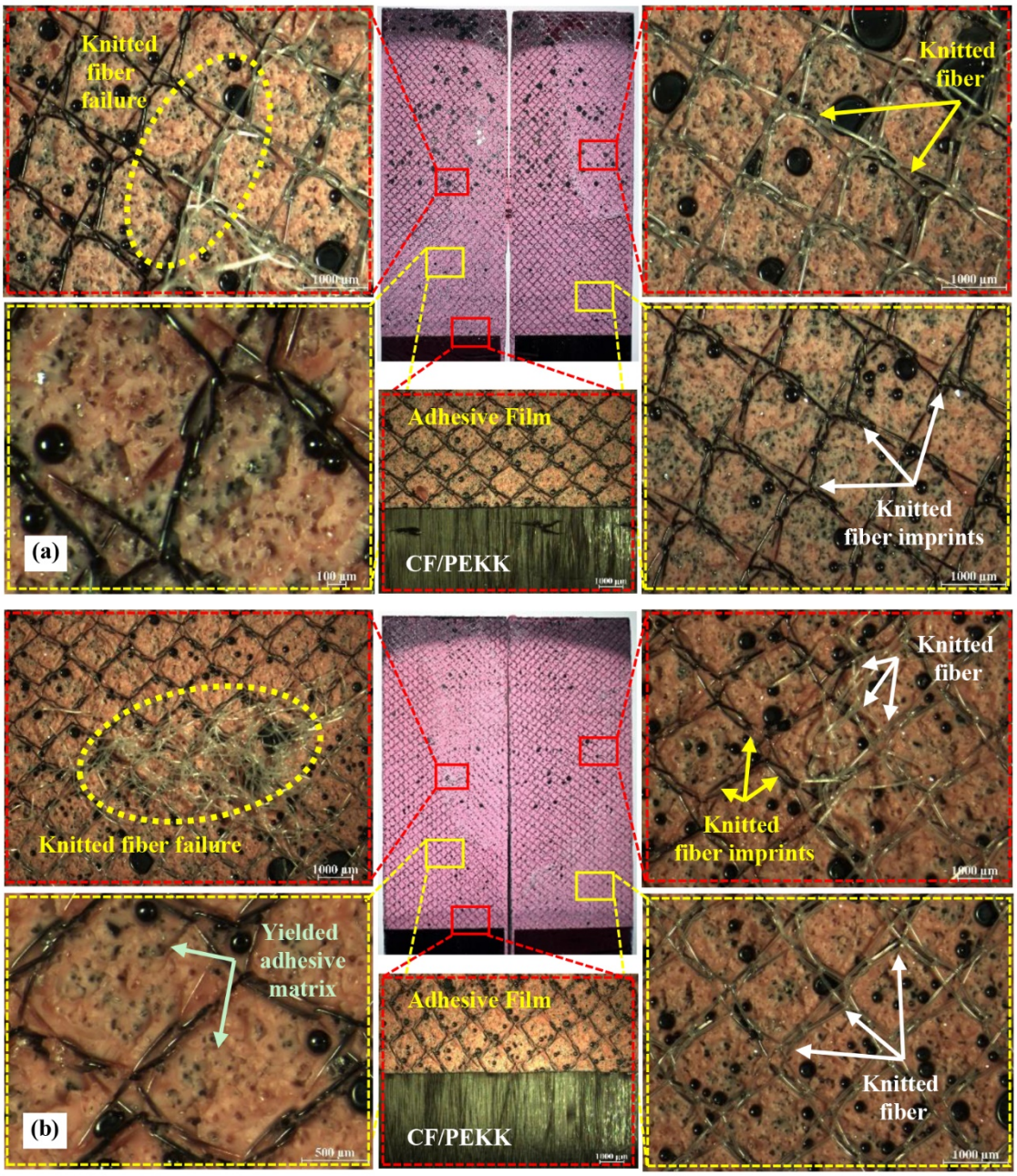

Figure 5 Fractographic failure analysis of conditioned ABJs using stereo microscopy (a) RT, (b) HT.

Nevertheless, the fracture surface analysis of LT specimens leads to the conclusion that the failure type is predominantly ADH with partial cohesive damage in the forms of both thick-layer adhesive peeling and thin-

layer adhesive peeling (**Figure 6a**). It is clearly seen that there are two arrest lines on the fracture surface of LT-conditioned specimens, and these lines are attributed to load drops as shown in **Figure 2a**. Additionally, brittle adhesive cracking is observed, attributed to the cryogenic temperatures that increase the brittleness of both the adhesive and the matrix polymers. Thereby, contrary to RT- and HT-conditioned specimens, there is almost no KFFs as seen in **Figure 6a**. However, complementary observations between stereo microscopy images and AE findings could not be established for LT specimens. Specifically, the identification of C4 failure, with a 60.06% distribution from AE inspection, differs from the COH failures observed in RT and HT specimens. This lack of correlation is further addressed and resolved through detailed SEM analysis in the upcoming section, which corroborates the AE findings.

For the CHT-conditioned specimen, the fracture surface microscopy addresses similar behavior with the RT and HT samples. However, the fracture surface analysis of CHT specimens highlights the dominance of COH, characterized by knitted fiber imprints, as shown in **Figure 6b.** Additionally, it is clear that there is partial brittle MC in AF. Adhesive residue fragments are also observed inside the damaged knitted fibers due to the brittleness caused by CHT conditioning introducing thermal residual stress. Thereby, CHT conditioning may produces COH and MC failures, but MC can become dominant due to cyclic thermal exposure including moisture [38]. These conclusions from microscopy images are supported with the AE inspection with maximum percentage distributions of COH (C4) and MC (C1) at 53.82% and 34.81% (**Figure 4d)**.

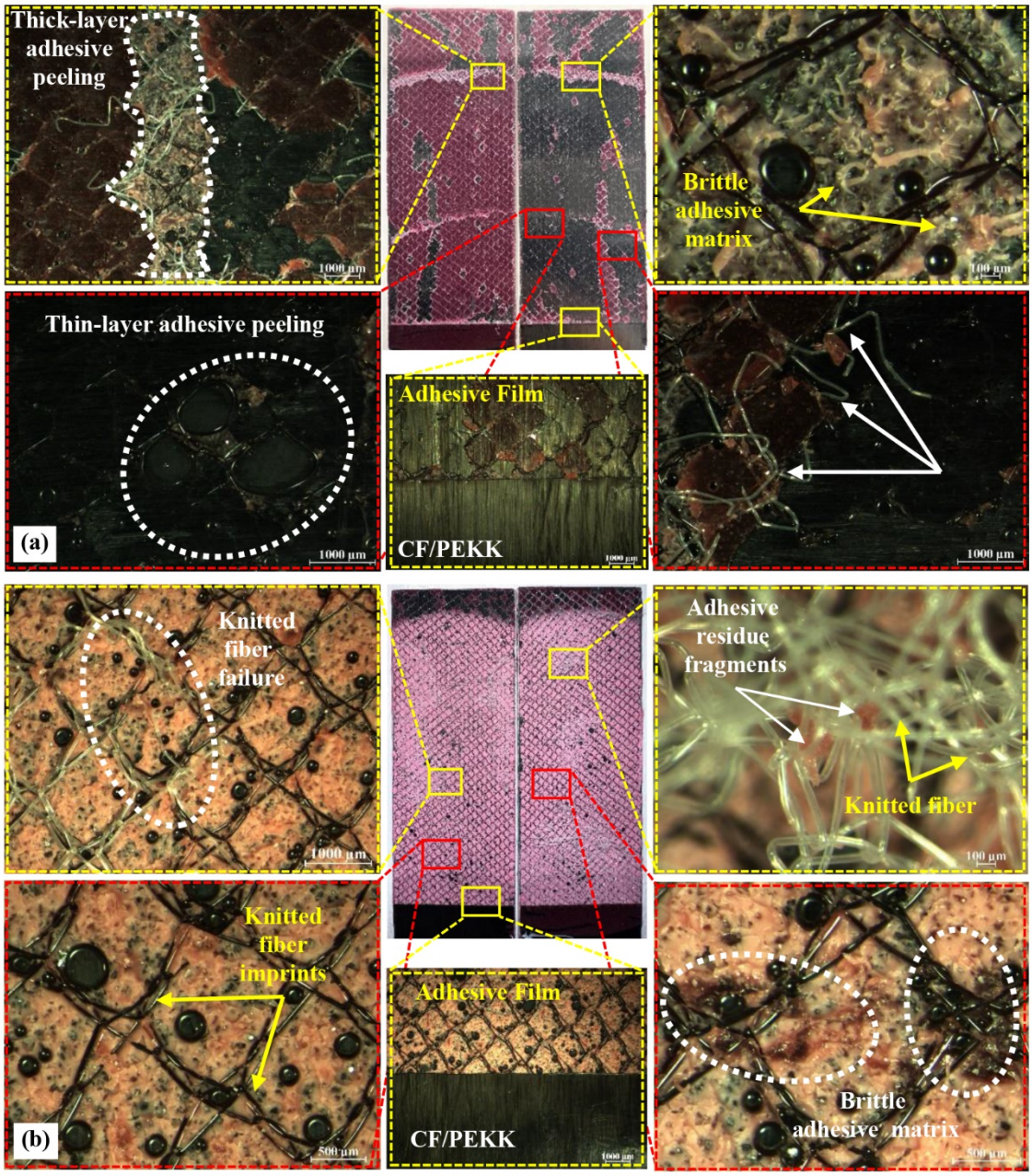

Figure 6 Fractographic failure analysis of conditioned ABJs using stereo microscopy (a) LT and (b) CHT.

Finally, the comprehensive understanding of mode-I fracture behavior is enhanced by SEM analyses of all specimen sets. A detailed examination of the fractured surface of ABJs tested under RT conditions is provided in **Figure 7** and **Supplementary Figure S3**. It is evident that, although not observable in stereo microscope images (**Figure 5a**), there are locally smooth surfaces attributed to ADH in RT-conditioned specimens, as shown in **Figure 7a**. Notably, debonding and knitted fiber imprints are also present on the surface. Despite the presence of ADH in localized areas, COH is prevalent across the fracture surface (see **Figure 7b**). During the mode-I fracture toughness tests, the crack progressed within the AF due to the strong adhesion between the adhesive and adherend. As seen in **Figure 7c**, knitted fiber imprints are visible on the fractured surfaces, indicating the fibers' good

bridging capabilities. This allows them to separate from one side without breaking while remaining attached to the other surface. On the other hand, when knitted fibers exceed their load-bearing capacity, they may break due to increasing deformation. Following this rupture, the fibers may accumulate on top of one another as seen in **Figure 7d**. It is apparent that knitted fibers undergo low plastic deformation and rupture, carrying adhesive debris with them during the debonding.

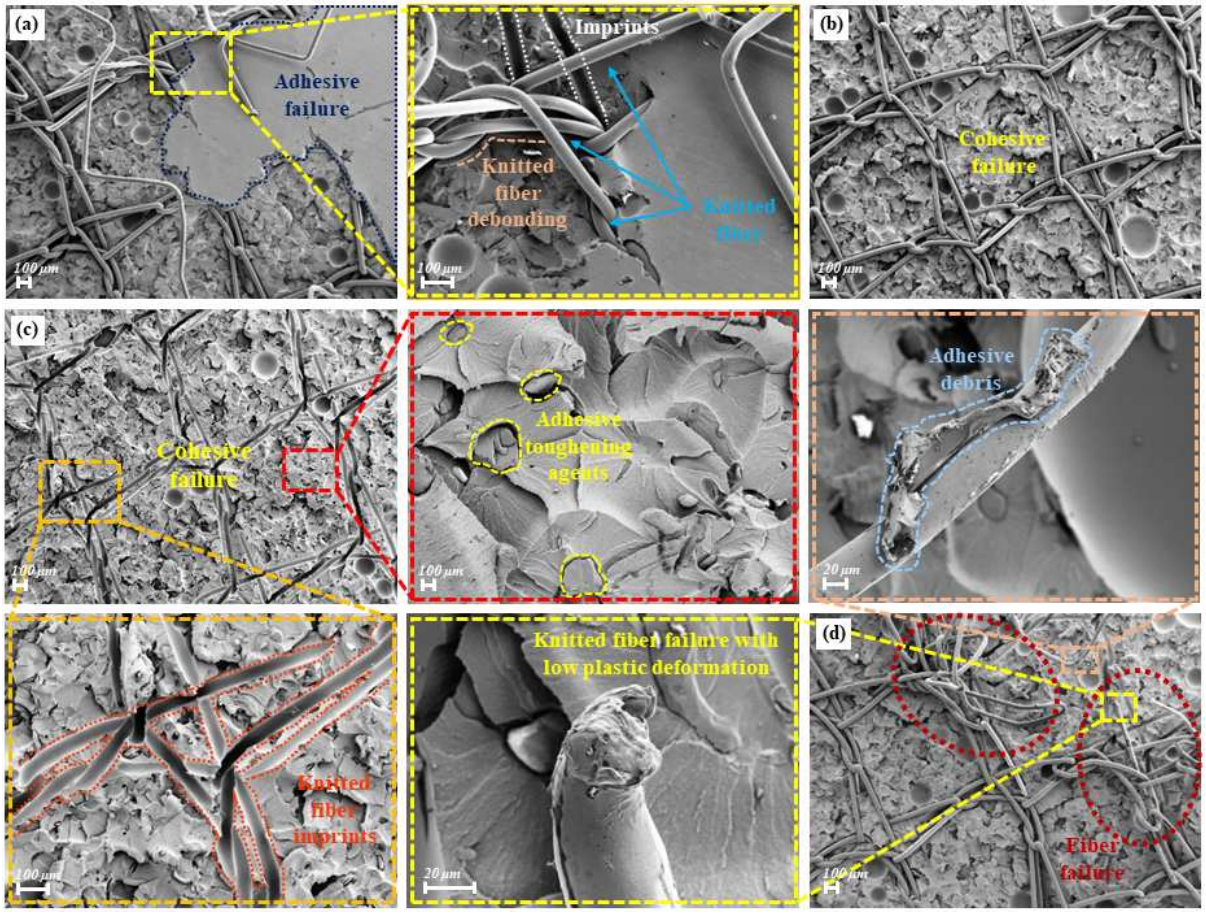

Figure 7 Dominant failures of the fractured surface of RT-conditioned ABJs; (a) ADH, (b) COH, (c) knitted fiber debonding and COH, and (d) KFFs

SEM images of the fractured surface of HT-conditioned ABJs are given in **Figure 8**. Similar to RT-conditioned specimens, the dominant failure is COH in HT-conditioned ones as shown in **Figure 8a**. However, debonding between the adhesive matrix and knitted fibers is more pronounced in HT-conditioned specimens compared to RT-conditioned ones. Additionally, HT causes structural deformation in the knitted fibers, resulting in damage characterized by layer splitting. In contrast to RT-conditioned specimens, the knitted fibers become ductile and thus undergo high plastic deformation (see in **Figure 8b**). This high plastic deformation changes the shape of damaged knitted fibers compared to RT-conditioned specimens, displaying characteristics of ductile breakage, such as stacking more on top of each other. It is obviously seen in **Figure 8c** knitted fiber imprints occur

on the fractured surface like RT-specimens. However, the toughening agents, which are commonly used in aerospace grade AF [43], yield with the HT effect or debond from the adhesive polymer due to the CTE difference (**Supplementary Figure S4**).

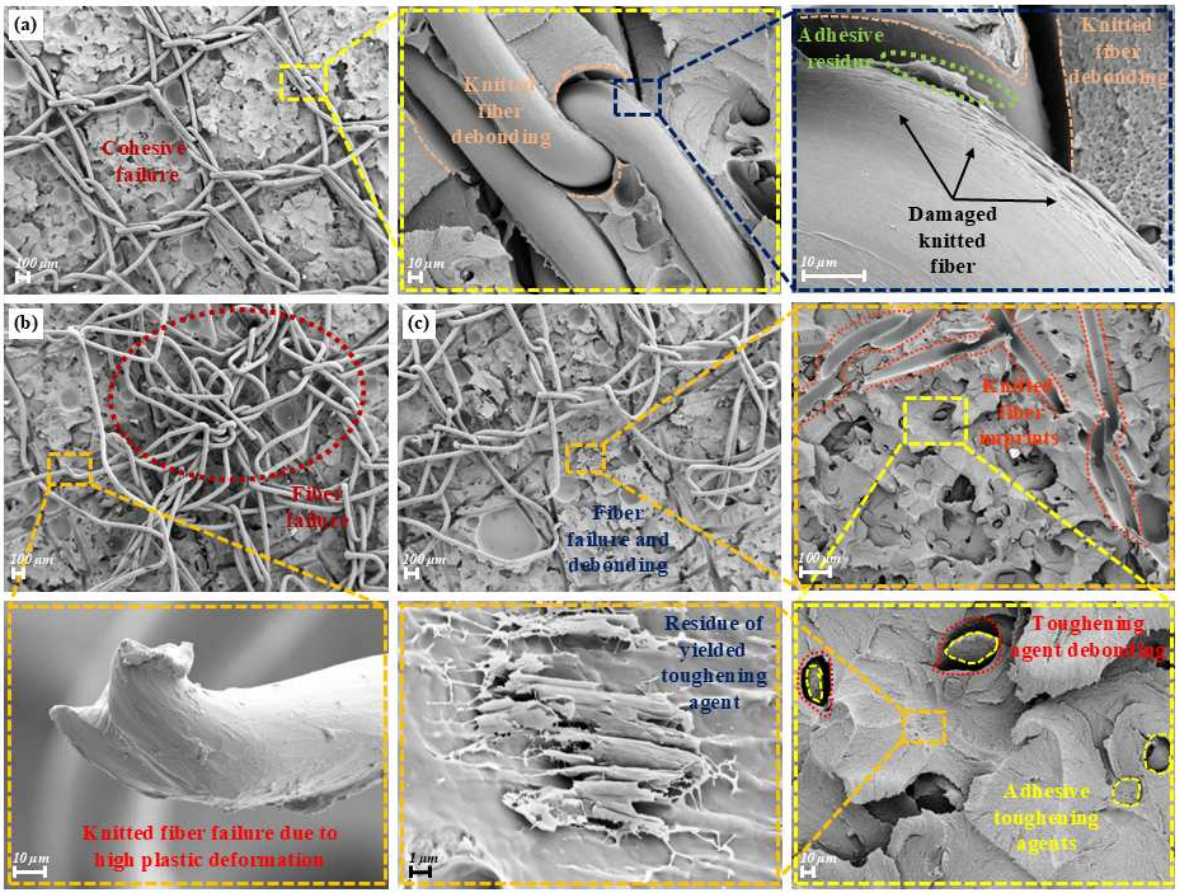

Figure 8 Dominant failures of the fractured surface of HT-conditioned ABJs; (a) COH, (b) KFFs, (c) knitted fiber debonding

Figure 9 shows the SEM images of the fractured surface of conditioned under LT. The key finding is that the dominant failure type is not COH unlike the RT- and HT-conditioned specimens. The fractured surface has partial COH region, but, there are ADH region on the surface as seen in **Figure 9a**. Moreover, due to the brittleness of adhesive matrix, adhesive debris are visible on the surface of knitted fibers. Unlike the HT-conditioned specimens, toughening agents are not highly affected by the LT exposure; yielding does not occur, and instead, brittle fracture of the toughening agents is observed. There is a discrepancy between the AE findings and the stereo microscope images for LT specimens, as the anticipated damage detected by AE cannot be visually confirmed through the stereo microscope. In this context, the SEM image in **Figure 9b** reveals the LFT on the fractured surface, which results from the residual stresses [15], thereby confirming the AE findings. Moreover, knitted fibers exhibit brittle breakage at LT, in contrast to the high plastic deformation observed at HT. As a consequence of weakened adhesion at the fiber-matrix interface caused by cryogenic-induced matrix brittleness

(**Supplementary Figure S5**), mechanisms such as fiber-matrix delamination triggering LFT [24,42]. This results in the top ply of CF/PEKK composite delamination, leading to peeled CF region and CF imprints on the fractured surface. Also, during this splitting, the CF ruptures are observed (see in **Figure 9c**).

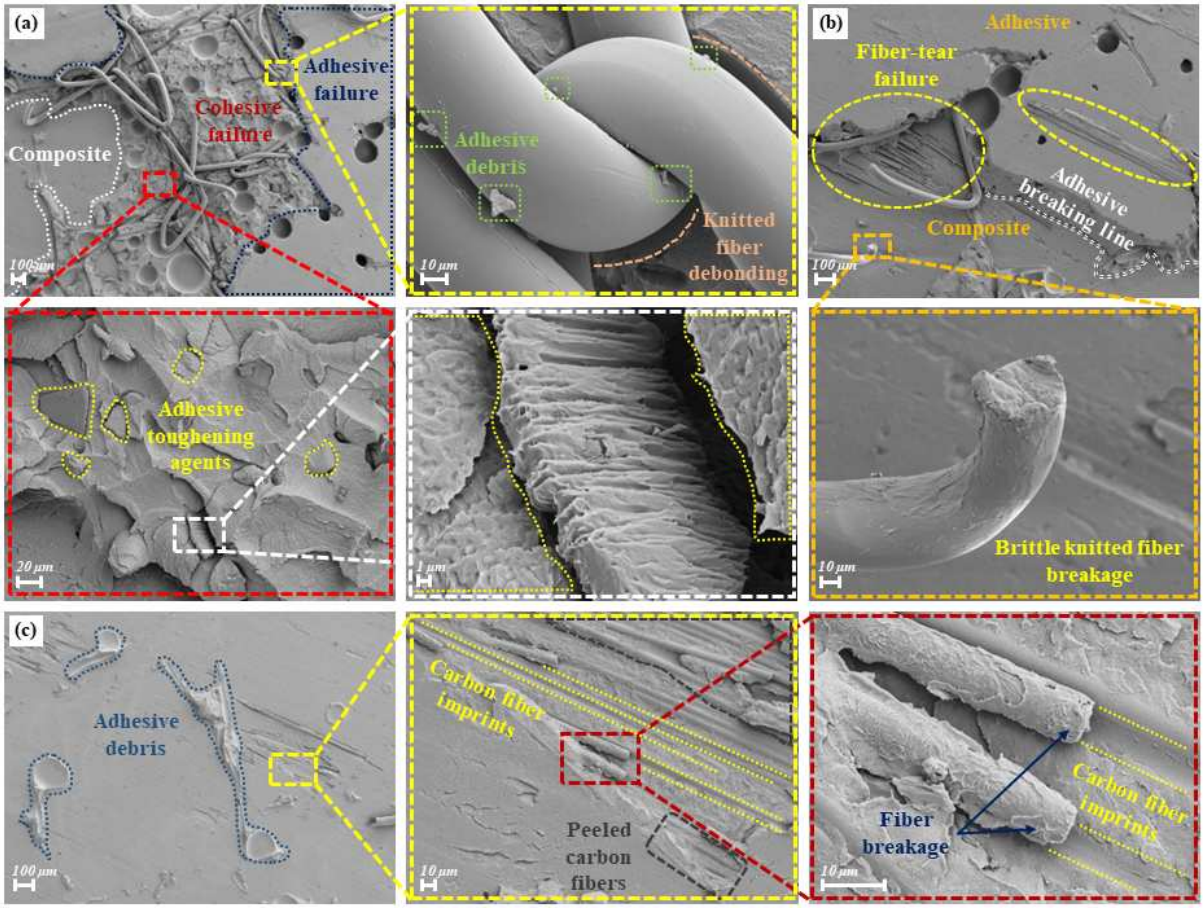

Figure 9 Dominant failures of the fractured surface of LT-conditioned ABJs; (a) ADH & COH (b) LFT, (c) CF failure.

A detailed SEM examination of conditioned under CHT is given in **Figure 10**. It is evident that the predominant failure under this condition is COH. As seen in **Figure 10a**, adhesive toughening agents are less affected by thermal cycling as much as RT- and HT-conditioned samples. The moisture exposure at HT affects the raptured knitted fiber morphology resulting in extreme deformation, as seen in **Figure 10b**. Additionally, moisture triggers the plasticization and swelling in both adhesive matrix and composite laminates matrix, weakening the interface between the adhesive and the knitted fibers. This leads to the formation of LFT and debonding of knitted fibers, as detailed in **Figure 10c**. Due to the plasticization effect of moisture, the adhesive matrix is also severely deformed (**Supplementary Figure S6**), resulting in shear cusps formation. Also, by reason of the weakened interface, CFs are separated from the composite laminate surface, while polymer yielding occurs simultaneously in the plasticized matrix. However, degradation of the interface between the adhesive and the adherends leads to ADH, as seen in **Figure 10d**.

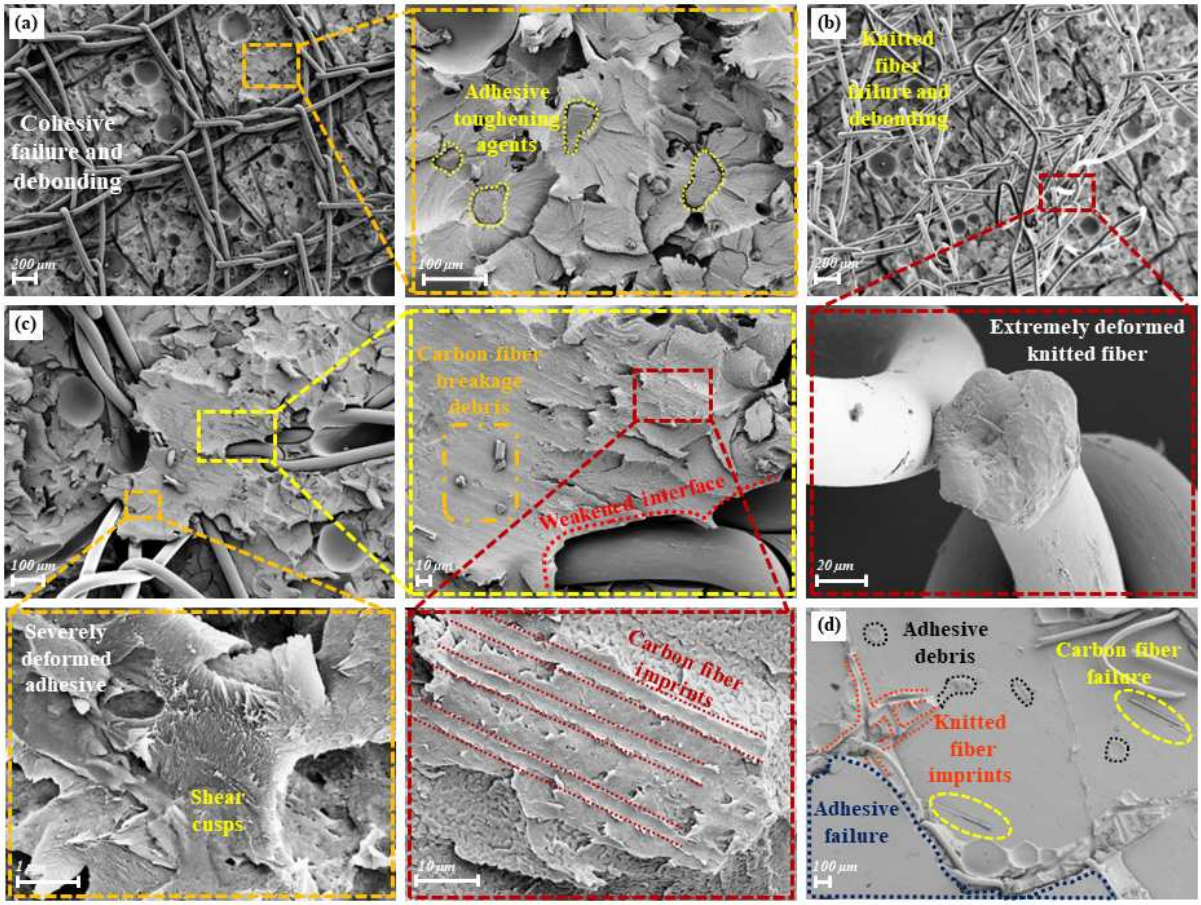

Figure 10 Dominant failures of the fractured surface of CHT-conditioned ABJs; (a) COH & knitted fiber debonding, (b) KFFs, (c) LFT and (d) ADH.

3.2 Sliding Mode (mode-II) Results

The load–displacement curves of ABJs under sliding mode for different environmental conditions are shown in **Figure 11a**. As expected, the conditioned samples at cryogenic environment reveal improved mode-II delamination resistance than other conditioned counterparts. The higher mode-II (shear mode) fracture toughness observed at LT for composite joints, compared to mode-I (tensile opening) fracture toughness, can be attributed to the distinct mechanisms of crack propagation and the influence of material and interfacial properties under these conditions. Opening mode (mode-I) involves the separation of layers or fibers perpendicular to the plane of the joint [31]. At LT, the resin matrix often becomes more brittle due to reduced ductility and increased stiffness [9,42,44]. This brittleness results in a decreased ability to absorb energy, lowering the mode-I fracture toughness. On the other hand, sliding mode (mode-II) involves shear deformation and interfacial sliding [32]. Energy dissipation mechanisms (crack paths) such as microcracking, interfacial debonding, fiber bridging, and frictional sliding are pronounced in mode-II fractures [45]. These mechanisms enhance energy absorption, contributing to higher fracture toughness by improving resistance to crack growth under shear loading. At LT, the brittle resin may increase interfacial friction and energy dissipation during crack propagation in Mode-II, leading to higher

resistance. Consequently, the load required to propagate a crack in Mode-II testing is likely higher for LT-conditioned specimens. Conversely, HT-conditioned specimens exhibit stable ductile-like behavior at higher temperatures, allowing pre-cracks to propagate more easily within the adhesive film without deflecting into the interface region. This results in lower load-carrying capacities compared to other conditioned samples [20]. For the CHT sample, the findings from the mode-I investigation, which highlight the weakening of interfacial bonding strength due to moisture exposure, are believed to also contribute to a decrease in mode-II test performance [42,46]. The mean values of the mode-II fracture toughness for the all-test sets are compared in **Figure 11b**. It is clear that the LT-conditioned group has higher mode-II values than other counterparts. As expected, CHT leads to a decrease in the fracture toughness of the ABJs, but exhibits lower behavior than RT but higher than HT.

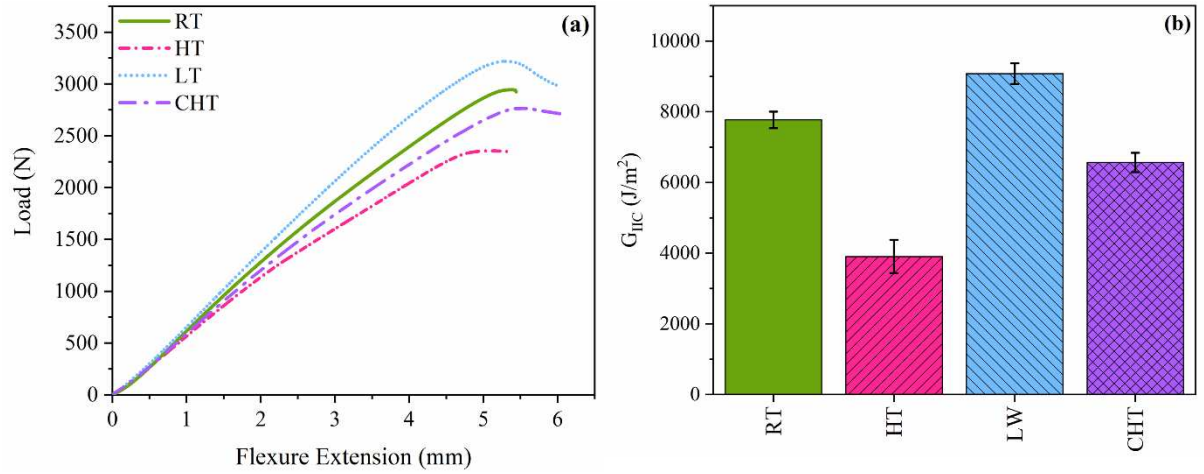

Figure 11 Mode-II fracture toughness properties of ABJs for different environmental conditions a) load-flexure extension and b) Comparison of mean G_{IIC}.

3.3 Dynamic-mechanical Analysis of ABJs

The dynamic-mechanical behavior under three-point bending mode of ABJs under different environmental conditions is illustrated in **Figure 12**. The average values of storage modulus data with standard deviation for ABJs under different conditions at various temperature are provided in **Figure 12a**, with inset bar charts. It is observed that the storage modulus values are generally at highest levels when conditioned at LT, due to the increased rigidity of the ABJ caused by the tight packing arrangement of the molecules. In the HT-conditioned specimens, the loose packing of the structure leads to easier polymer chain mobility, a higher degree of the relaxation of the thermal stresses and lower intermolecular bond strengths, reducing the storage modulus [47]. Since CHT conditions involve a combination of LT, HT, and moisture effects, the impact on dynamic-mechanical behavior is more intricate. The moisture to which ABJs are exposed weakens the strength of the adhesive layer with plasticization and also causes localized adhesion deficiencies at the adhesive-adherend interface with blistering [48]. Simultaneously, cyclic temperature induces residual stresses in the ABJ. Thus, the combination of

these effects results in storage modulus values for CHT that fall between those of LT and HT, as seen in **Figure 12a**. Furthermore, as shown in the inset bar chart in **Figure 12a**, all specimens exhibit a consistent order of storage modulus values as the temperature changes. The first and second peaks observed in the tan delta-temperature curves, given in **Figure 12b,** represent the T_g of the AF [49] and CF/PEKK composite [30], respectively. It is observed that temperature exposures during environmental conditioning (HT and LT) do not significantly affect the T_g of either the adhesive or the adherend, likely due to the short exposure time of the specimens. However, specimens conditioned with CHT show a decrease in T_g for the AF due to both prolonged exposure time to temperature conditioning and presence of high humidity in the environment. The results indicate that the combination of temperature and relative humidity directly influences the AF's T_g, as highlighted in the literature [48].

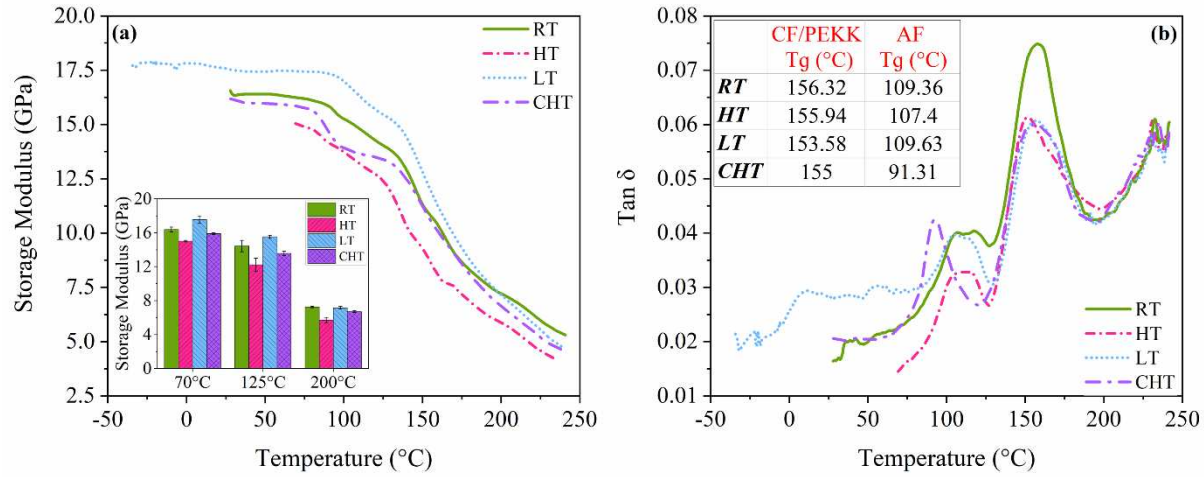

Figure 12 Storage modulus-temperature and b) tan-δ versus temperature curves of ABJs for different conditioned.

The slope of the linear part of the load-displacement curves in **Figure 11a** recorded of mode-II fracture tests is related to the bending stiffness of the bonded parts. On the other hand, the storage modulus values obtained in dynamic mechanical analyses provide information about the elastic character and rigidity of the material [37]. It is worth noting here that the effect of different environmental condition exposures on the stiffness behavior of the samples exhibited a similar trend in both analyses.

4. Conclusion

This novel study is one of the first to comprehensively and comparatively investigate the performance of CF/PEKK thermoplastic composite joints under various environmental conditions. It provides valuable insights into the fundamental interactions influencing the mechanical and fracture behavior of thermoset-based adhesive bonds. Key findings are given as follows.

Mode-I fracture test results indicate that specimens conditioned at RT, HT, and CHT exhibit more stable crack propagation compared to those conditioned at LT, which show sharp peaks indicative of unstable crack growth. HT conditioning enhances adhesive ductility, leading to smoother crack propagation but reduced delamination resistance. CHT specimens present intermediate load values and reduced delamination resistance compared to RT specimens, yet still outperform HT specimens.

AE analyses and fractographic evaluations reveal that environmental conditions significantly impact failure modes and AE activity in ABJs. High temperatures promote cohesive failure (COH) due to the polymer's increased ductility. Conversely, LT conditions lead to lower AE activity and higher rates of light fiber tear failure (LFT). Thermal cycling intensifies material degradation and hygroscopic effects, increasing COH and LFT due to weakened fibers and interfaces.

Interestingly, LT conditions notably improve mode-II delamination resistance due to increased bending stiffness and matrix brittleness, requiring higher loads to propagate the crack. In contrast, HT conditions result in reduced mode-II delamination resistance due to ductile behavior within the adhesive film. CHT-conditioned specimen, influenced by moisture exposure, exhibit weakened interfacial bonding and further reduced mode-II performance.

Dynamic mechanical analysis (DMA) reveals the highest storage modulus values under LT conditions, attributed to increased rigidity. HT conditions result in lower modulus values due to looser molecular packing, which enhances polymer chain mobility but weakens intermolecular bonds. CHT conditions, which combine effects of temperature cyclic and moisture, result in intermediate storage modulus values and decreased glass transition temperature (T_g) of adhesive film, highlighting the complex interplay of temperature and humidity on ABJ mechanical properties.

Overall, this study highlights the critical impact of environmental conditions on the fracture and dynamic mechanical performance of CF/PEKK adhesively bonded joints (ABJs). The combined effects of environmental conditioning and loading configuration significantly alter ABJ performance. Thus, these key findings will establish a framework for understanding and optimizing the performance of adhesive bonded joints (ABJs) in aerospace applications, contributing to design criteria that ensure reliability and effectiveness under diverse and harsh environmental conditions. Future studies may incorporate fatigue loading under harsh environmental conditions to simulate repetitive loading scenarios in aerospace applications.

Acknowledgments

The authors gratefully acknowledge financial support from the Scientific and Technological Research Council of Turkey (TÜBİTAK) with project number 221M565 and 218M709.

Data availability

Data will be made available on request.

References

[1] Siddique A, Iqbal Z, Nawab Y, Shaker K. A review of joining techniques for thermoplastic composite materials. J Thermoplast Compos Mater 2023;36:3417–54. https://doi.org/10.1177/08927057221096662.

[2] Ageorges C, Ye L, Hou M. Advances in fusion bonding techniques for joining thermoplastic matrix composites: A review. Compos - Part A Appl Sci Manuf 2001;32:839–57. https://doi.org/10.1016/S1359-835X(00)00166-4.

[3] Kaybal HB, Ulus H. Comparative analysis of thermoplastic and thermoset adhesives performance and the influence on failure analysis in jointed elium-based composite structures. Polym Compos 2024;45:3474–92. https://doi.org/10.1002/pc.28003.

[4] Yudhanto A, Alfano M, Lubineau G. Surface preparation strategies in secondary bonded thermoset-based composite materials: A review. Compos Part A Appl Sci Manuf 2021;147:106443. https://doi.org/10.1016/j.compositesa.2021.106443.

[5] Yildirim C, Ulus H, Beylergil B, Al-Nadhari A, Topal S, Yildiz M. Effect of atmospheric plasma treatment on Mode-I and Mode-II fracture toughness properties of adhesively bonded carbon fiber/PEKK composite joints. Eng Fract Mech 2023;289:109463. https://doi.org/https://doi.org/10.1016/j.engfracmech.2023.109463.

[6] Yildirim C, Ulus H, Beylergil B, Al-Nadhari A, Topal S, Yildiz M. Tailoring adherend surfaces for enhanced bonding in CF/PEKK composites: Comparative analysis of atmospheric plasma activation and conventional treatments. Compos Part A Appl Sci Manuf 2024;180:108101. https://doi.org/10.1016/j.compositesa.2024.108101.

[7] Ulus H, Burak Kaybal H. Out-of-plane static loading performance of lightweight aluminum/composite FML structures for retrofitting applications: Effectiveness of bonded, bolted and hybrid bonded/bolted joining techniques under hydrothermal aging environment. Constr Build Mater 2023;403:133124. https://doi.org/10.1016/j.conbuildmat.2023.133124.

[8] Wang X, Hou Z, Yang Y. A Study on the Aging Resistance of Injection-molded Glass Fiber Thermoplastic Composites. Fibers Polym 2022;23:502–14. https://doi.org/10.1007/s12221-021-0449-4.

[9] Mára V, Michalcová L, Kadlec M, Krčil J, Špatenka P. The effect of long-time moisture exposure and low temperatures on mechanical behavior of open-hole Cfrp laminate. Polym Compos 2021;42:3603–18. https://doi.org/10.1002/pc.26082.

[10] Treml AE, Gouvêa RF, Sales RCM, Donadon M V., Shiino MY, Bressan JD. Anti-symmetrical curved composite laminate subject to delamination induced by thermal cycling. Fatigue Fract Eng Mater Struct 2017;40:1072–85. https://doi.org/10.1111/ffe.12565.

[11] Rahmani A, Choupani N. Experimental and numerical analysis of fracture parameters of adhesively bonded joints at low temperatures. Eng Fract Mech 2019;207:222–36. https://doi.org/10.1016/j.engfracmech.2018.12.031.

[12] Budhe S, Banea MD, de Barros S, da Silva LFM. An updated review of adhesively bonded joints in composite materials. Int J Adhes Adhes 2017;72:30–42. https://doi.org/10.1016/J.IJADHADH.2016.10.010.

[13] Loh WK, Crocombe AD, Abdel Wahab MM, Ashcroft IA. Environmental degradation of the interfacial fracture energy in an adhesively bonded joint. Eng Fract Mech 2002;69:2113–28. https://doi.org/10.1016/S0013-7944(02)00004-8.

[14] Sukur EF, Elmas S, Seyyednourani M, Eskizeybek V, Yildiz M, Sas HS. A rational study on the hydrothermal aging of AFP manufactured CF/polyetherketoneketone composites with in situ consolidation supported by acoustic emission inspection. J Appl Polym Sci 2022;139:e52480. https://doi.org/10.1002/app.52480.

[15] Viana G, Costa M, Banea MD, Da Silva LFM. A review on the temperature and moisture degradation of adhesive joints. Proc Inst Mech Eng Part L J Mater Des Appl 2017;231:488–501.

https://doi.org/10.1177/1464420716671503.
[16] Nunes PDP, Marques EAS, Carbas RJC, Akhavan-Safar A, da Silva LFM. Quasi-static and intermediate test speed validation of SHPB specimens for the determination of mode I, mode II fracture toughness of structural epoxy adhesives. Eng Fract Mech 2022;262:108231. https://doi.org/10.1016/j.engfracmech.2021.108231.
[17] Wagih A, Tao R, Yudhanto A, Lubineau G. Improving mode II fracture toughness of secondary bonded joints using laser patterning of adherends. Compos Part A Appl Sci Manuf 2020;134:105892. https://doi.org/10.1016/j.compositesa.2020.105892.
[18] Banea MD, Da Silva LFM, Campilho RDSG. Mode II fracture toughness of adhesively bonded joints as a function of temperature: Experimental and numerical study. J. Adhes., vol. 88, 2012, p. 534–51. https://doi.org/10.1080/00218464.2012.660835.
[19] Banea MD, Da Silva LFM, Campilho RDSG. Effect of temperature on tensile strength and mode i fracture toughness of a high temperature epoxy adhesive. J Adhes Sci Technol 2012;26:939–53. https://doi.org/10.1163/156856111X593649.
[20] Ashcroft IA, Hughes DJ, Shaw SJ. Mode I fracture of epoxy bonded composite joints: 1. Quasi-static loading. Int J Adhes Adhes 2001;21:87–99. https://doi.org/10.1016/S0143-7496(00)00038-5.
[21] Yoshimura A, Takaki T, Noji Y, Yokozeki T, Ogasawara T, Ogihara S. Fracture toughness of CFRP adhesive bonded joints at cryogenic temperature. J Adhes Sci Technol 2012;26:1017–31. https://doi.org/10.1163/156856111X593694.
[22] Melcher RJ, Johnson WS. Mode I fracture toughness of an adhesively bonded composite-composite joint in a cryogenic environment. Compos Sci Technol 2007;67:501–6. https://doi.org/10.1016/j.compscitech.2006.08.026.
[23] Abdel-Monsef S, Renart J, Carreras L, Maimí P, Turon A. Effect of environmental conditioning on pure mode I fracture behaviour of adhesively bonded joints. Theor Appl Fract Mech 2020;110:102826. https://doi.org/10.1016/j.tafmec.2020.102826.
[24] Brito CBG, Sales RCM, Donadon M V. Effects of temperature and moisture on the fracture behaviour of composite adhesive joints. Int J Adhes Adhes 2020;100:102607. https://doi.org/10.1016/j.ijadhadh.2020.102607.
[25] Katsiropoulos C V., Chamos AN, Tserpes KI, Pantelakis SG. Fracture toughness and shear behavior of composite bonded joints based on a novel aerospace adhesive. Compos Part B Eng 2012;43:240–8. https://doi.org/10.1016/j.compositesb.2011.07.010.
[26] Teixeira de Freitas S, Zarouchas D, Poulis JA. The use of acoustic emission and composite peel tests to detect weak adhesion in composite structures. J Adhes 2018;94:743–66. https://doi.org/10.1080/00218464.2017.1396975.
[27] Droubi MG, Stuart A, Mowat J, Noble C, Prathuru AK, Faisal NH. Acoustic emission method to study fracture (Mode-I, II) and residual strength characteristics in composite-to-metal and metal-to-metal adhesively bonded joints. J Adhes 2018;94:347–86. https://doi.org/10.1080/00218464.2017.1278696.
[28] Lima RAA, Tao R, Bernasconi A, Carboni M, Teixeira de Freitas S. Acoustic emission approach for identifying fracture mechanisms in composite bonded Joints: A study on varying Substrate's stacking sequence. Theor Appl Fract Mech 2024;132:104490. https://doi.org/10.1016/j.tafmec.2024.104490.
[29] Liu R, Shen GT, Zhang PF, Zhou W. Acoustic emission response and progressive failure behaviors of composite adhesively bonded joints loaded by Mode i and II. Mater Res Express 2019;7:15307. https://doi.org/10.1088/2053-1591/ab5c3b.
[30] Yildirim C, Tabrizi IE, Al-Nadhari A, Topal S, Beylergil B, Yildiz M. Characterizing damage evolution of CF/PEKK composites under tensile loading through multi-instrument structural health monitoring techniques. Compos Part A Appl Sci Manuf 2023;175:107817. https://doi.org/https://doi.org/10.1016/j.compositesa.2023.107817.
[31] ASTM D5528-13. Standard test method for mode I interlaminar fracture toughness of unidirectional fiber-reinforced polymer matrix composites. ASTM Int 2014;03:1–12.
[32] ASTM 7905/ D7905M-14. Standard Test Method for Mixed Mode I-Mode II Interlaminar Fracture Toughness of Unidirectional Fiber Reinforced Polymer Matrix Composites. ASTM Int 2006;08:1–6.
[33] ASTM D1002-10. Standard Test Method for Apparent Shear Strength of Single-Lap-Joint Adhesively Bonded Metal Specimens by Tension Loading. ASTM Int 2010;01:10–5.
[34] Seyyednourani M, Akgun S, Ulus H, Yildiz M, Sas HS. Experimental investigation on Compression-After-Impact (CAI) response of aerospace grade thermoset composites under low-temperature conditions assisted with acoustic emission monitoring. Compos Struct 2023;321:117260. https://doi.org/10.1016/j.compstruct.2023.117260.
[35] EN ISO 9142. Adhesives - Guide to selection of standard laboratory ageing conditions for testing bonded joints. Int Organ Stand 2003.
[36] Sukur EF, Elmas S, Eskizeybek V, Sas HS, Yildiz M. An experimental implication of long-term hot-

wet-aged carbon fiber/polyether ketone ketone composites: The impact of automated fiber placement process parameters and process-induced defects. J Appl Polym Sci 2023;140:e54076. https://doi.org/10.1002/app.54076.
[37] Ulus H, Kaybal HB, Cacık F, Eskizeybek V, Avcı A, Burak H, et al. Fracture and dynamic mechanical analysis of seawater aged aluminum-BFRP hybrid adhesive joints. Eng Fract Mech 2022;268:108507. https://doi.org/10.1016/j.engfracmech.2022.108507.
[38] Markatos DN, Tserpes KI, Rau E, Markus S, Ehrhart B, Pantelakis S. The effects of manufacturing-induced and in-service related bonding quality reduction on the mode-I fracture toughness of composite bonded joints for aeronautical use. Compos Part B Eng 2013;45:556–64. https://doi.org/10.1016/j.compositesb.2012.05.052.
[39] Dong C, Li K, Jiang Y, Arola D, Zhang D. Evaluation of thermal expansion coefficient of carbon fiber reinforced composites using electronic speckle interferometry. Opt Express 2018;26:531. https://doi.org/10.1364/oe.26.000531.
[40] Mahato KK, Shukla MJ, Kumar DS, Ray BC. In- service Performance of Fiber Reinforced Polymer Composite in Different Environmental Conditions: A Review. J Adv Res Manuf Mater Sci Metall Eng 2014;1:55–88.
[41] Hohe J, Neubrand A, Fliegener S, Beckmann C, Schober M, Weiss KP, et al. Performance of fiber reinforced materials under cryogenic conditions—A review. Compos Part A Appl Sci Manuf 2021;141:106226. https://doi.org/10.1016/j.compositesa.2020.106226.
[42] Wei Y, Jin X, Luo Q, Li Q, Sun G. Adhesively bonded joints – A review on design, manufacturing, experiments, modeling and challenges. Compos Part B Eng 2024;276:111225. https://doi.org/10.1016/j.compositesb.2024.111225.
[43] Al-Nadhari A, Yildirim C, Topal S, Emami Tabrizi I, Yildiz M. In-situ acoustic emission based technique for damage detection and identification and failure mode prediction in scarf repaired composite structures. Meas J Int Meas Confed 2025;242:116068. https://doi.org/10.1016/j.measurement.2024.116068.
[44] Hartwig G, Knaak S. Fibre-epoxy composites at low temperatures. Cryogenics (Guildf) 1984;24:639–47. https://doi.org/10.1016/0011-2275(84)90083-3.
[45] Oshima S, Mamishin A, Hojo M, Nishikawa M, Matsuda N, Kanesaki M. High-resolution in situ characterization of micromechanisms in CFRP laminates under mode II loading. Eng Fract Mech 2022;260:108189. https://doi.org/10.1016/j.engfracmech.2021.108189.
[46] Abdel-Monsef S, Renart J, Carreras L, Turon A, Maimí P. Effect of environment conditioning on mode II fracture behaviour of adhesively bonded joints. Theor Appl Fract Mech 2021;112:102912. https://doi.org/10.1016/j.tafmec.2021.102912.
[47] Marques EAS, Da Silva LFM, Banea MD, Carbas RJC. Adhesive joints for low- and high-temperature use: An overview. J Adhes 2014;91:556–85. https://doi.org/10.1080/00218464.2014.943395.
[48] Mendonça Sales R de C, Brito CBG, Silveira NNA, de Souza Sena JL, Arbelo MA, Donadon MV, et al. Hygrothermal effects on mode II interlaminar fracture toughness of co-bonded and secondary bonded composites joints. Polym Compos 2019;40:3220–32. https://doi.org/10.1002/pc.25176.
[49] Technical Datasheet AF 163-2 Structural Adhesive Film. Scotch-Weld 3M 2009:21.